Electronic Supplementary Information (ESI)

Emergence of high piezoelectricity along with robust electron mobility in Janus structures in semiconducting Group IVB dichalcogenide monolayers

1. Bader population charge analysis on atomic species

Table S1. Effective charges on atomic species calculated via Bader population analysis

MX2	M	X	X
ZrS_2	+2.0505	-1.0259	-1.0246
$ZrSe_2$	+1.8635	-0.9316	-0.9318
$ZrTe_2$	+1.564	-0.7818	-0.7822
HfS_2	+2.2439	-1.1244	-1.1195
$HfSe_2$	+2.0522	-1.029	-1.0233
$HfTe_2$	+1.7396	-0.8696	-0.8700

MXY	M	X	Y
ZrSSe	+1.9452	-1.0538	-0.8913
ZrSTe	+1.8023	-1.0858	-0.7165
ZrSeTe	+1.7241	-0.9676	-0.7565
HfSSe	+2.1343	-1.1476	-0.9866
HfSTe	+1.9477	-1.1623	-0.7854
HfSeTe	+1.8789	-1.0483	-0.8306

Red: semi-conducting, Blue: metallic **(based on GGA-PBE)**

2. Electronic band gap and band dispersion

Table S2. Electronic band gap of monolayer MX_2 (M = Zr, Hf; X= S, Se, Te) using GGA+PBE and HSE06 functional.

	ZrS_2	$ZrSe_2$	$ZrTe_2$	ZrSSe	ZrSeTe	ZrSTe
GGA+PBE	1.16	0.38	-0.52	0.66	-0.04	-0.12
HSE06	1.99	1.07	-0.13	1.37	0.43	0.30

	HfS_2	$HfSe_2$	$HfTe_2$	HfSSe	HfSeTe	HfSTe
GGA+PBE	1.33	0.48	-0.3	0.74	-0.03	-0.23
HSE06	2.03	1.16	0.13	1.45	0.44	0.15

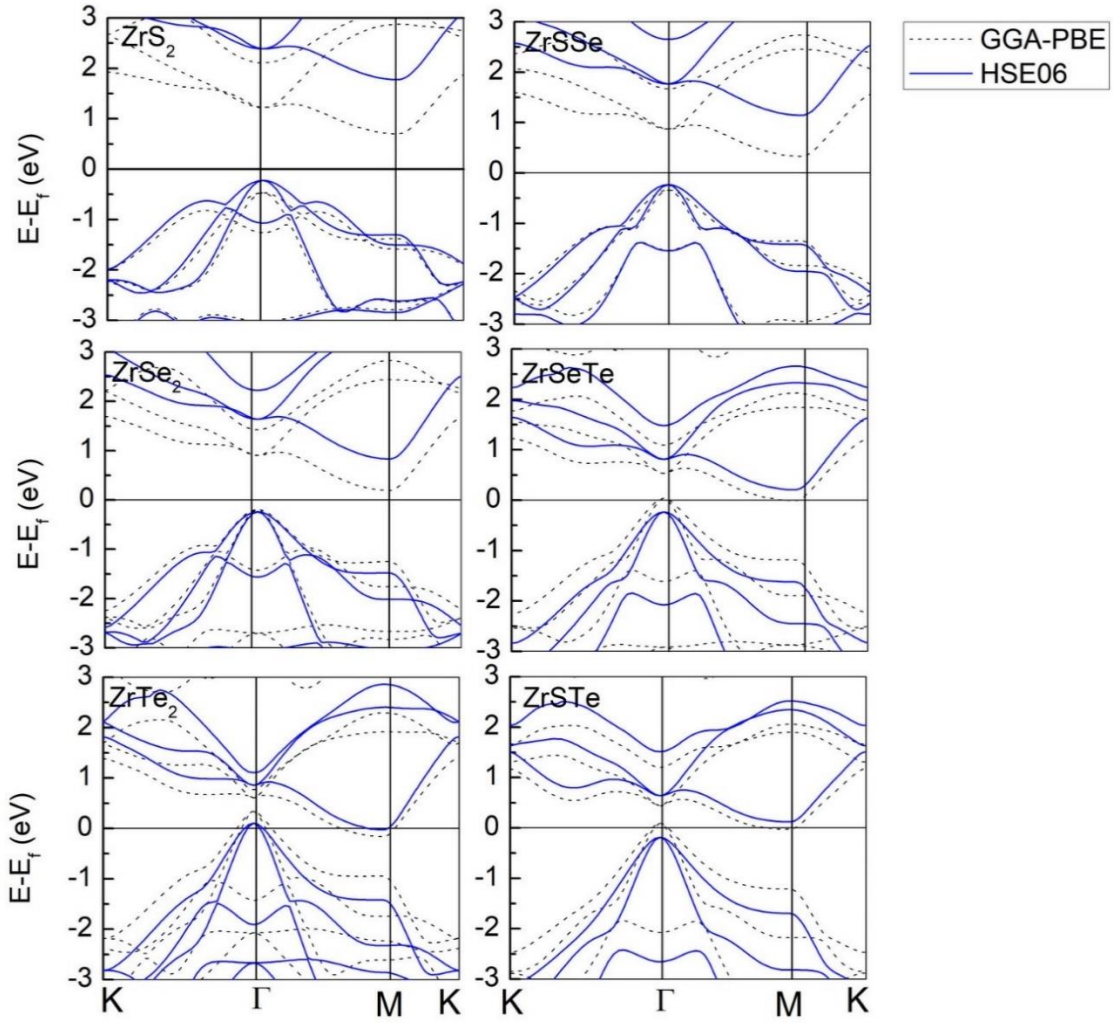
ZrS2
ZrSSe
ZrSe2
ZrSeTe
ZrTe2
ZrSTe
GGA-PBE
HSE06
E-Ef (eV)
K
Γ
M
K

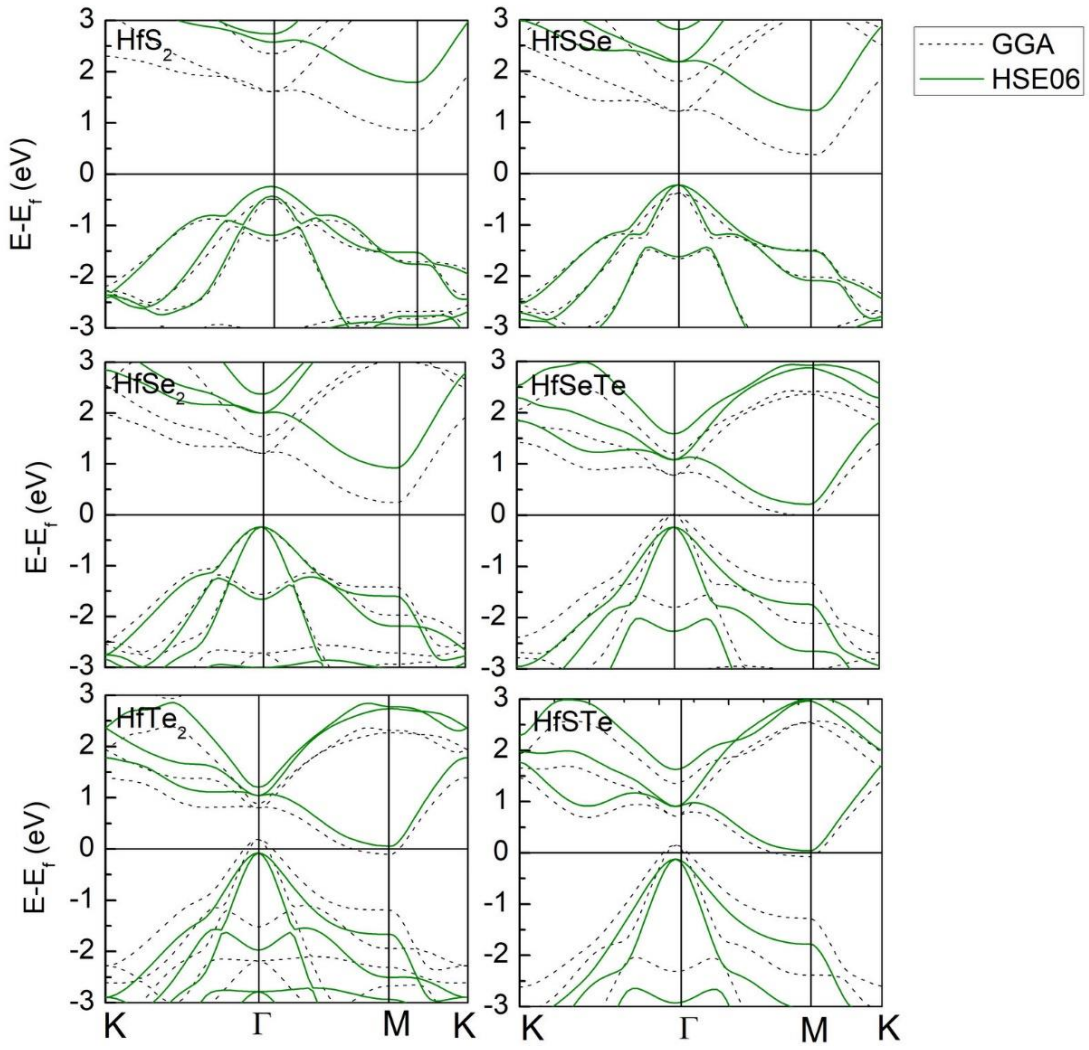

Fig S3 Electronic band dispersion of 1T-MX_2 and their corresponding Janus MXY monolayers determined via GGA-PBE (dotted curves) and HSE06 calculations (solid curves). M= Zr, Hf and X=S/Se/Te.

3. Dynamical stability

Even if the total energy of a structure is minimized, its stability cannot be assured. Therefore, frequencies of the vibrational modes of optimized single-layer MX_2 or MXY in 1T or Janus structures have been calculated along the high-symmetry k-points in the BZ to provide a rigorous test for the stability. A structure is taken to be stable only when calculated frequencies of all phonon modes in the BZ are positive; otherwise, imaginary frequencies indicate instability. In such calculations, the long wavelength, out of plane acoustical (ZA) modes are vulnerable to instability. Thus, caution has to be taken in calculating forces with extreme accuracy.

To confirm the dynamical stability, phonon dispersions of 1T-MX_2 and their Janus MXY monolayers have been calculated by using the density functional perturbation theory (DFPT). The results are plotted in Fig. S4 for all Janus MXY and also for 1T-MX_2 monolayers. No appreciable imaginary vibrational frequency is noticed in the first Brillouin zone, which clearly suggests that monolayers are dynamically stable. Except a small pocket near the Γ point, no trace of imaginary frequencies is observed in the Brillouin zone. This small pocket of instability is extremely sensitive to the details of the calculation and in some cases, it disappears altogether. This suggests that it merely indicates the difficulty in achieving numerical convergence for the flexural phonon branch, which appears to be a common issue in the first principle calculations for 2D materials [Phys. Rev. B 89, 205416 (2014)]. The existence of small regions of phonon instability in the flexural acoustic (ZA) modes around the Γ point has also been observed in graphene, silicone, molybdenum disulfide and gallium chalcogenides. The region of instability shows extreme sensitivity to simulation parameters such as supercell size and k-point sampling. Moreover, the absolute values of the imaginary frequencies are close to zero and vary by the amount by which the acoustic branches of the dispersion curve miss zero when Newton's third law is not imposed on the matrix of the force constants. For these reasons, it is understood that these regions of instability are spurious. [Phys. Rev. B 89, 205416 (2014)]

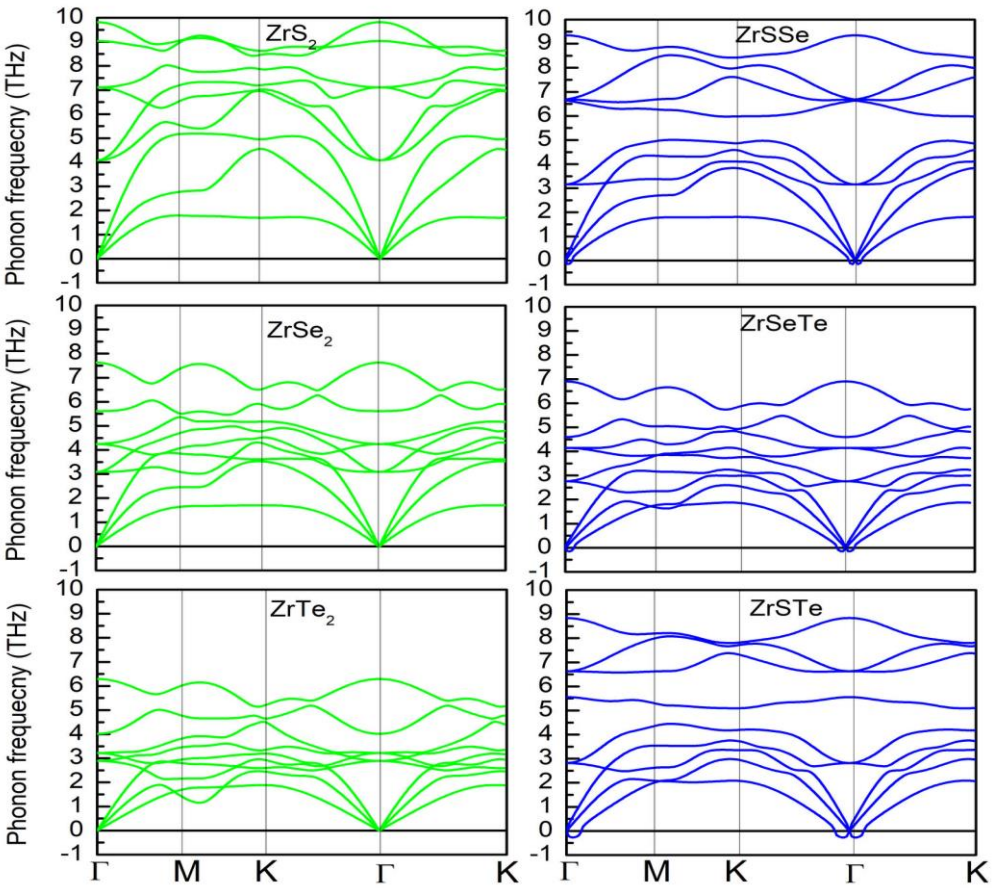
ZrS2
ZrSSe
ZrSe2
ZrSeTe
ZrTe2
ZrSTe
Phonon frequecny (THz)
Γ M K Γ K

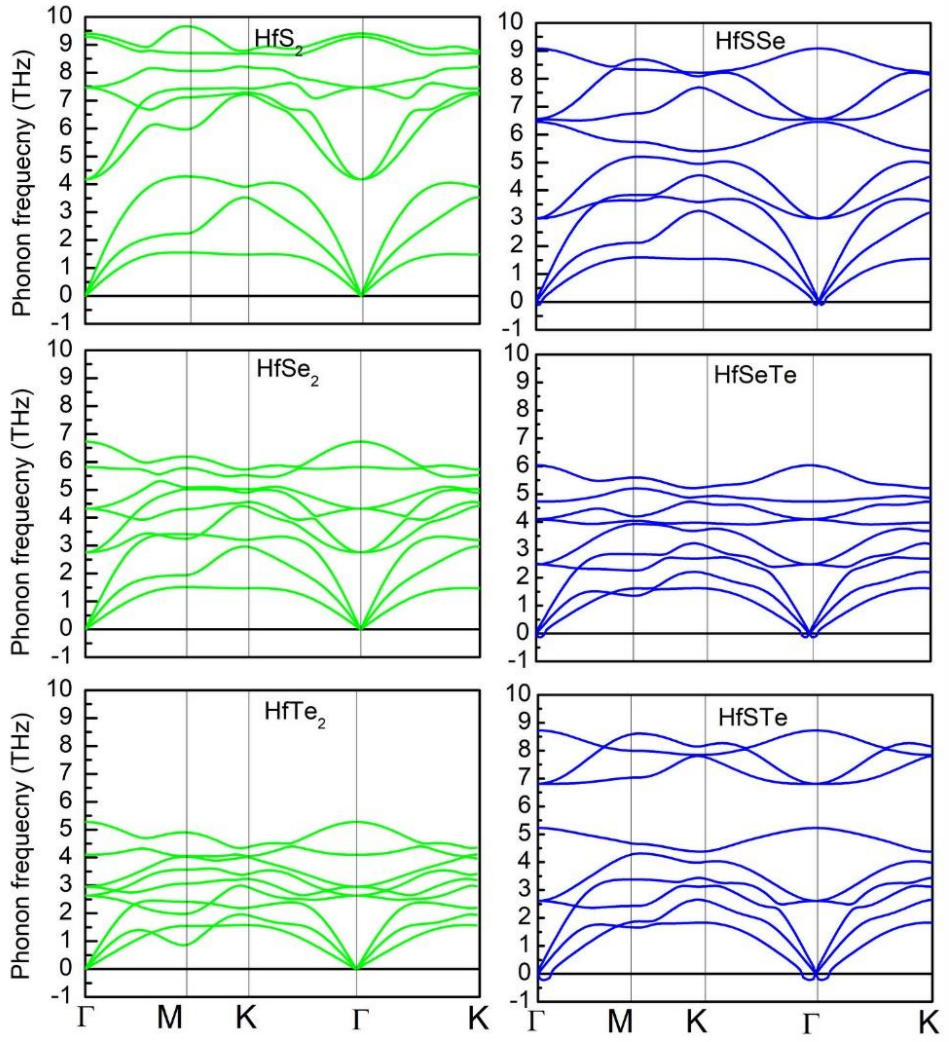

Figure S4. Phonon energy dispersion spectrum of 1T-MX_2 and MXY Janus monolayers.

4. Determination of piezoelectric strain coefficients, d_{il}

The piezoelectric strain coefficients can be determined by equating each element of 6x6 matrix, using eq. 1, 2 and 3 in eq. 4 [The boxed equations can be found in main text of this article].

1. $e_{15} = d_{15}C_{44} - d_{22}C_{14}$
2. $-e_{22} = d_{15}C_{14} - 2d_{22}\left(\frac{C_{11}-C_{12}}{2}\right)$

$$\boxed{d_{22} = \frac{e_{22}}{C_{11} - C_{12}}}$$

3. $-e_{22} = -d_{22}C_{11} + d_{22}C_{12} + d_{15}C_{13}$

$$\boxed{d_{22} = \frac{e_{22}}{C_{11} - C_{12}}}$$

4. $e_{22} = -d_{22}C_{12} + d_{22}C_{11} - d_{15}C_{14}$

$$\boxed{d_{22} = \frac{e_{22}}{C_{11} - C_{12}}}$$

5. $e_{15} = -d_{22}C_{14} - d_{22}C_{14} + d_{15}C_{44}$
6. $e_{31} = d_{31}C_{11} + d_{31}C_{12} + d_{33}C_{13}$

$$\boxed{d_{31} = \frac{e_{31}}{C_{11} + C_{12}}}$$

7. $e_{31} = d_{31}C_{12} + d_{31}C_{11} + d_{33}C_{13}$

$$\boxed{d_{31} = \frac{e_{31}}{C_{11} + C_{12}}}$$

8. $e_{33} = d_{31}C_{13} + d_{31}C_{13} + d_{33}C_{33}$

N.A. The above relations have been calculated on the basis of finite C_{ij} values. $C_{11} = C_{22} \neq 0$, $C_{12} = C_{21} \neq 0$, $C_{66} = \frac{C_{11} - C_{12}}{2} \neq 0$. Specifically, $C_{14} = -C_{24} = C_{56} = C_{65} \approx 0$; and hence, neglected. Also, $C_{33} \approx 0$ and $C_{44} = 0$.

5. Born effective charges

Table S5. Born effective charge tensor on each ionic species in 2D monolayer nanosheets (2D-NS)

$2D-NS$	M_{xx}	M_{yy}	M_{zz}	X_{xx}	X_{yy}	X_{zz}	Y_{xx}	Y_{yy}	Y_{zz}
ZrSSe	8.10	8.10	0.55	-4.26	-4.26	-0.31	-4.18	-4.18	-0.22
ZrSTe	6.13	6.13	0.35	-3.28	-3.28	-0.26	-2.78	-2.78	-0.06
ZrSeTe	6.86	6.86	0.40	-3.53	-3.53	-0.24	-3.19	-3.19	-0.11
HfSSe	7.64	7.64	0.57	-4.03	-4.03	-0.32	-3.97	-3.97	-0.23
HfSTe	6.75	6.75	0.37	-3.48	-3.48	-0.27	-3.32	-3.32	-0.08
HfSeTe	7.40	7.40	0.39	-3.80	-3.80	-0.25	-3.62	-3.63	-0.12

6. Mobility calculations

For a systematic investigation of the charge carrier mobility in semi-conducting monolayers along the two non-equivalent, in-plane, transverse directions, namely, zigzag (x) and armchair (y) directions, the primitive supercell having an inherent hexagonal symmetry has been purposefully converted into a supercell with a rectangular orthorhombic symmetry. For the calculation of the deformation potential, external mechanical strain of an infinitesimal magnitude (-0.5% to +0.5% uniaxial strain in step sizes of 0.2%) has been applied along the in-plane transverse directions, at a time.

Two formulation: [1] *Bardeen and Shockley* [*Physical Review*, 1950, **80**, 72–80] and [2] *Lang et al. [Physical Review B*, 2016, **94**, 235306] have been used in the present work in the calculation of longitudinal acoustic phonon limited charge carrier mobility.

$$\mu_{\alpha x}^{(1)} \approx \frac{2e\hbar^3 C_{x\_2D}}{3k_B T m_{\alpha x}^{*2} E_{\alpha x}^2} x10^4\ cm^2V^{-1}s^{-1}$$

$$\mu_{\alpha x}^{(2)} \approx \frac{e\hbar^3\left(\frac{5C_{x_{2D}}+3C_{y_{2D}}}{8}\right)}{k_B T (m_{\alpha x})^{\frac{3}{2}}(m_{\alpha y})^{\frac{1}{2}}\left(\frac{9E_{\alpha x}^2+7E_{\alpha x}E_{\alpha y}+4E_{\alpha y}^2}{20}\right)} x10^4\ cm^2V^{-1}s^{-1}$$

Table S6. Parameters along the zigzag (x) and armchair (y) directions used in the carrier mobility calculations on different 2D monolayer nanosheets (2D-NS)

2D-NS	$m_e^*(x)$	$m_e^*(y)$	$C_{11}(x)$	$C_{11}(y)$	$E_e(x)$	$E_e(y)$	$\mu_e^{(2)}$(x)	$\mu_e^{(2)}$(y)	$\tau_e(x)$	$\tau_e(y)$	$\mu_e^{(1)}$(x)	$\mu_e^{(1)}$(y)
ZrS2	0.283	1.998	75.57	75.57	-3.71	-3.65	120.11	2.42	19.32	2.75	973.37	20.17
ZrSe2	0.187	1.813	68.86	68.86	-2.67	-3.66	597.66	5.64	63.54	5.82	3921.98	22.2
ZrSSe	0.24	2.21	70.32	70.32	3.57	3.33	186.53	2.25	25.45	2.83	1360.07	18.43
ZrSeTe	0.138	2.122	47.77	47.77	-5.56	-5.36	278.96	1.19	21.88	1.44	1152.1	5.24
ZrSTe	0.194	4.101	39.57	39.57	-4.05	-5.79	56.60	0.11	6.243	0.25	910.11	0.99
HfS2	0.238	2.382	80.77	80.77	2.82	2.83	308.36	3.07	41.72	4.16	2545.9	25.23
HfSe2	0.164	2.11	75.07	75.07	2.56	2.58	1195.79	7.20	111.50	8.64	6047.04	35.96
HfSSe	0.197	2.407	77.88	77.88	2.73	2.72	556.85	3.73	62.37	5.11	3823.07	25.79
HfSeTe	0.145	3.039	54.76	54.76	3.34	3.32	520.56	1.18	42.91	2.05	3314.96	7.63
HfSTe	0.151	4.085	51.51	51.51	4.15	4.22	205.10	0.27	17.60	0.64	1862.45	2.46

2D-NS	$m_h^*(x)$	$m_h^*(y)$	$C_{11}(x)$	$C_{11}(y)$	$E_h(x)$	$E_h(y)$	$\mu_h^{(2)}$(x)	$\mu_h^{(2)}$(y)	$\tau_h(x)$	$\tau_h(y)$	$\mu_h^{(1)}$(x)	$\mu_h^{(1)}$(y)
ZrS2	0.443	0.445	75.57	75.57	-8.69	-4.54	37.87	47.36	9.54	11.98	72.4	262.88
ZrSe2	0.28	0.28	68.86	68.86	-10.25	-4.56	167.08	221.25	26.59	35.22	118.69	599.74
ZrSSe	0.33	0.332	70.32	70.32	-9.52	-4.46	195.84	356.94	36.74	67.37	101.16	455.38
ZrSeTe	0.124	0.124	47.77	47.77	-6.04	-4.45	6740.51	7559.98	475.21	532.99	1209.15	2227.59
ZrSTe	0.111	0.111	39.57	39.57	-4.04	-5.59	11604.15	10274.14	732.34	648.40	2793.84	1459.28
HfS2	0.469	0.47	80.77	80.77	-8.81	-3.62	34.64	46.70	9.238	12.48	67.17	396.17
HfSe2	0.321	0.321	75.07	75.07	-6.6	-5.59	179.99	191.70	32.85	34.98	237.47	331.03
HfSSe	0.375	0.376	77.88	77.88	-6.74	-7.15	80.50	78.29	17.16	16.73	173.09	152.99
HfSeTe	0.191	0.192	54.76	54.76	-6.18	-8.96	741.95	639.23	80.57	69.78	558.03	262.71
HfSTe	0.147	0.148	51.51	51.51	-7.37	-7.68	1906.56	1851.60	159.34	155.80	623.11	566.09

7. Effects of external strain

In unstrained Janus monolayers, the elastic stiffness constants and piezoelectric constants are found to be isotropic. However, external mechanical strain is found to bring about anisotropy in them. This anisotropy in the elastic constants gives rise to a slight anisotropy in Young's modulus and Poisson's ratio, as follows:

$$Y_{zz(ac)} = Y_{11(22)} = \frac{C_{zz}C_{ac} - C_{12}^2}{C_{zz(ac)}} = \frac{C_{11}C_{22} - C_{12}^2}{C_{11(22)}}$$

$$\nu_{zz(ac)} = \nu_{11(22)} = \frac{C_{12}}{C_{zz(ac)}} = \frac{C_{12}}{C_{11(22)}}$$

where zz (ac) represent zig-zag (arm-chair) directions respectively

Table S7. Elastic stiffness constants, C_{11} (N/m), C_{22} (N/m). C_{12} (N/m), Young's modulus, Y_{2D} (N/m) & Poisson ratio,ν_{2D} along zig-zag (zz) and arm-chair (ac) directions, piezoelectric stress coefficients, e_{22} & e_{31} (10^{-10} C/m), piezoelectric strain coefficients, d_{22} & d_{31} (pm/V), external pressure, $P_{ext.}(GPa)$ and HSE06 band gap, E_g (eV) in unstrained and strained HfSSe monolayer: I and D denote indirect and direct band gap

HfSSe	C_{11}^{total}	C_{22}^{total}	C_{12}^{total}	Y_{zz}	Y_{ac}	ν_{zz}	ν_{ac}	e_{22}	e_{31}	d_{22}	d_{31}	$P_{ext.}$	$E_{g,HSE06}$
Unstrained	77.88	77.88	15.90	74.63	74.63	0.20	0.20	2.90	0.005	4.68	0.051	0	1.45 (I)
Uniaxial tensile along arm-chair at 9% strain	73.48	53.77	9.69	72.20	52.03	0.13	0.18	78.49	0.69	123.04	0.83	-2.8	1.61 (D)
Biaxial strain at 7% strain	55.22	54.15	10.79	53.11	51.99	0.19	0.20	16.74	0.14	37.67	0.21	-4.2	1.99 (D)

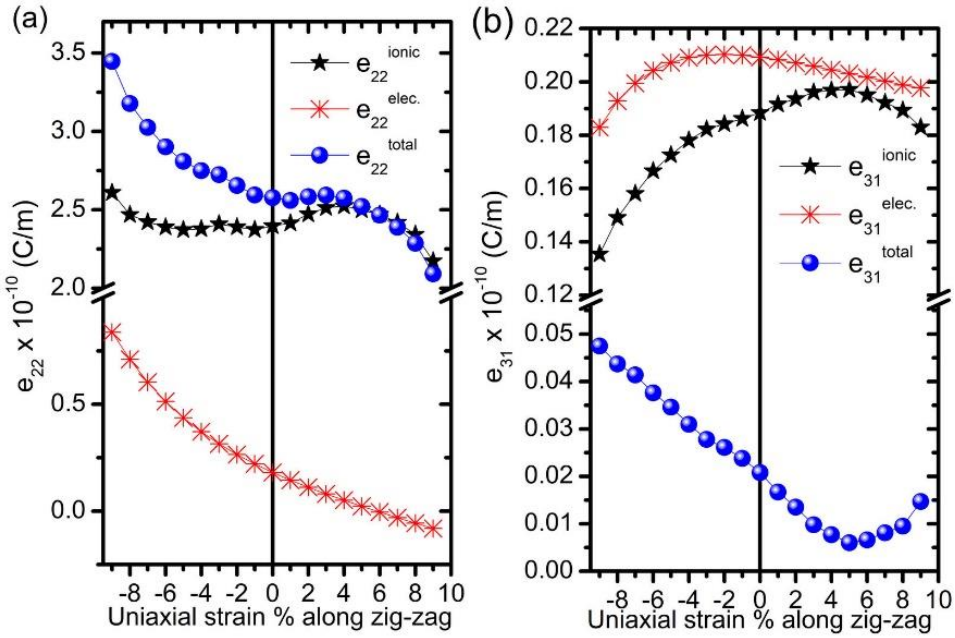

Fig. S5 Variation in (a) in-plane e_{22} and (b) out-of-plane e_{31} piezoelectric coefficients with the application of external mechanical strain along the zig-zag direction

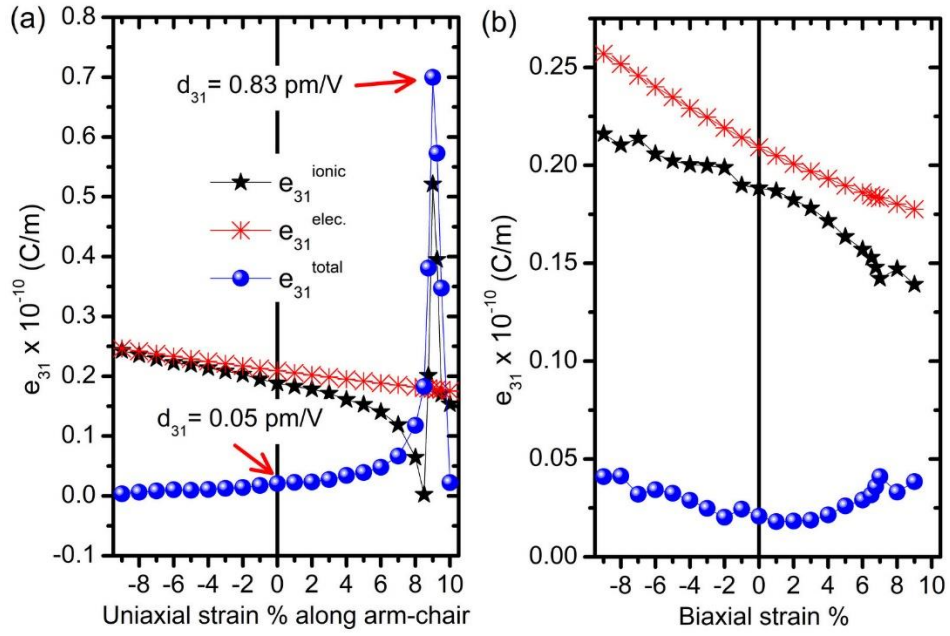

Fig. S6 Variation in the out-of-plane e_{31} piezoelectric coefficients with the application of (a) uniaxial strain along the arm-chair direction and (b) biaxial strain

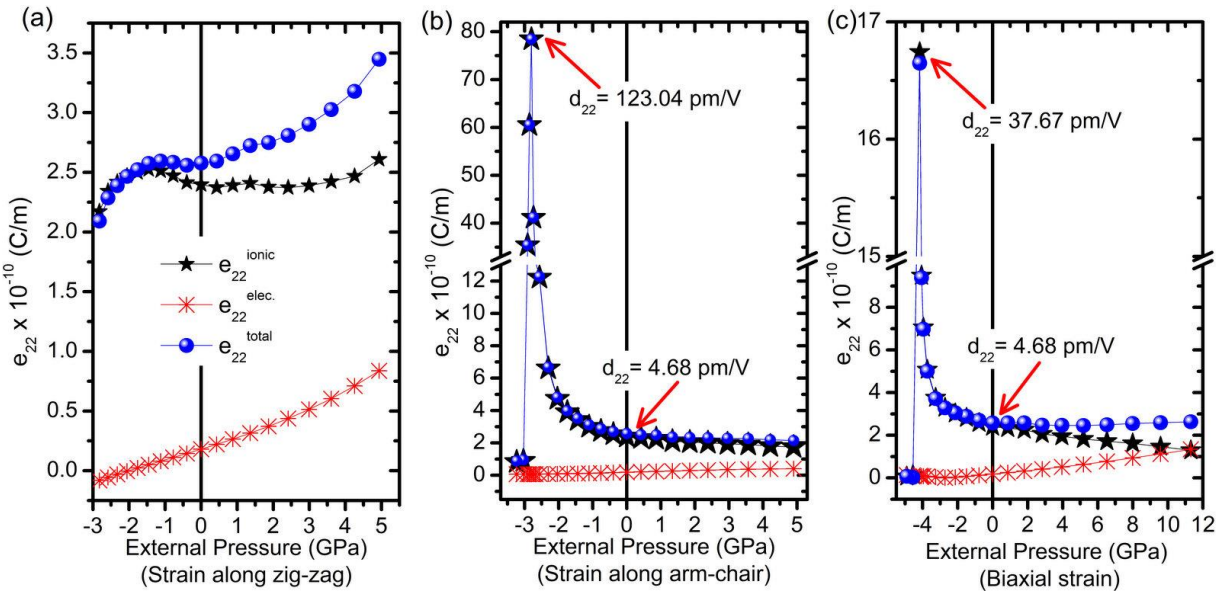

Fig. S7 Variation in the in-plane e_{22} piezoelectric coefficient with external pressure which is induced by the application of (a) uniaxial strain along the zig-zag and (b) arm-chair direction, and (c) biaxial strain

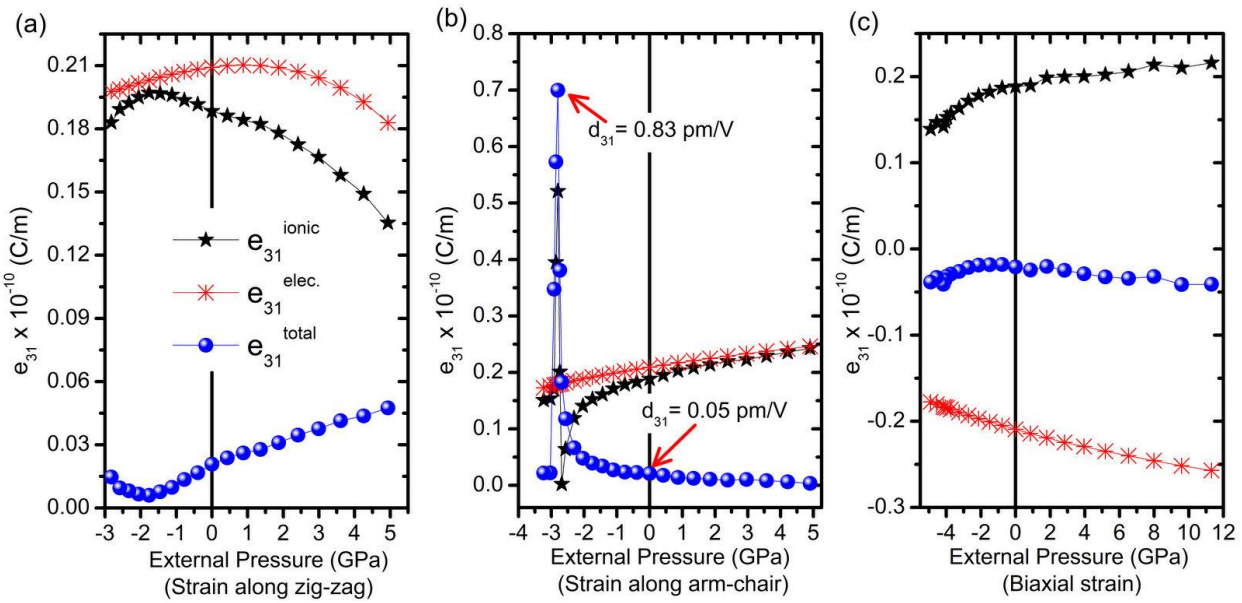

Fig. S8 Variation in the out-of-plane e_{31} piezoelectric coefficient with external pressure which is induced by the application of (a) uniaxial strain along zig-zag and (b) arm-chair direction, and (c) biaxial strain